# Real-time Monitoring of Asphalt Pavement Structure Fatigue Response Based on Tri-axis Accelerometer

## Abstract:

Manifestation of fatigue damage under repeated loads is considered one of the notable distresses of flexible asphalt pavements. However, monitoring the development process of such distresses in asphalt pavement in real-time especially through traditional fatigue prediction models remained a challenging task for researchers. In this paper, the self-developed sensing facility has been utilized to obtain the aggregate kinematic response signal (angle and acceleration) of the semi-circular specimen during the fatigue loading process in real-time, in the upper-middle (H/2), lower-middle (L/2) and lower-right (L/3) positions of the specimen. The variation characteristics of the angle and acceleration in the X, Y, and Z directions were analysed independently at three positions during the fatigue test. The correlation between the kinematic characteristic of the aggregate and the vertical deformation of the asphalt mixture specimen is established during the fatigue loading. The results illustrated that the asphalt mixture viscoelasticity attenuation during fatigue test caused the angle accumulation and acceleration response change of the specimen. The angle accumulation in the X-axis direction and acceleration variation in Y-axis direction of the aggregate at the H/2 position exhibited a significant three-stage change, which translated to the fatigue development process of asphalt mixture. The novel Angle-Accumulation Rate (AAR) of change is suggested as a long-term monitoring index for the fatigue development of the asphalt mixture which indicates occurring of macrocrack when the AAR reaches about ten times the inflection point of the AAR change curve. And the proposal of AAR index creatively combines the long-

term kinematic behaviour and mechanical behaviour of asphalt mixture, making long-term and real-time monitoring of the asphalt pavement health from the perspective of kinematics become possible.

**Keywords:** asphalt pavement; fatigue damage; sensor; angle; acceleration； real-time monitoring

# 1 Introduction

After the construction of asphalt pavement, the mechanical properties of asphalt mixture are attenuated under the repeated action of the long-term vehicle and environmental load, which leads to permanent structural deformation of asphalt pavement, and finally leads to structural damage or fatigue cracking of asphalt pavement (Wang *et al.* 2021). At present, fatigue failure has become the dominant failure mode of flexible asphalt pavement (Qiang *et al.* 2012, Guo *et al.* 2017, Liu *et al.* 2017).

Because the fatigue damage of asphalt pavement structure is affected by the size and frequency of the vehicle load, the temperature and humidity cycle of the environment, etc., it is difficult to predict the fatigue damage of asphalt pavement in the field. Therefore, the fatigue prediction of asphalt pavement is mainly focused on the indoor test. The commonly used laboratory test methods include the four-point bending fatigue test, indirect tensile test, trapezoidal cantilever test and so on. However, different test methods produce different results. Karami, LV, Yan, et al. studied the fatigue properties of asphalt mixtures using four-point bending, direct tensile and splitting fatigue tests separately. The results were quite different by different methods (Karami and Nikraz 2015, Lv *et al.* 2018, Yan *et al.* 2020). With the development of fatigue research, the application of Semi-Circular Bending (SCB) fatigue tests has increased. Hasan et al. compared and analysed the differences between four-point bending fatigue and SCB tests by studying the fatigue

properties of coarse and fine asphalt mixtures. The results showed significant differences in the fatigue properties of the two mixtures from the four-point bending test. In contrast, the SCB test results showed that the anti-fatigue properties of the two mixtures were similar (Hasan *et al.* 2019). However, Dong et al. found that SCB was more sensitive to stress ratio than splitting fatigue tests (Dong *et al.* 2020). In addition, after years of experimental research, researchers had a deeper understanding of the evolution of fatigue damage on asphalt pavement. They proposed various fatigue damage prediction models, which could be divided into the following categories: phenomenological, energy, and fracture mechanics (Kiplagat *et al.* 2017, Du *et al.* 2021). With the development of numerical simulation technology, researchers have proposed many new fatigue prediction models by combining numerical simulation technology and indoor fatigue test (Wang *et al.* 2018b). Wang et al. proposed an evaluation model of fatigue damage evolution based on continuum mechanics by the evolution law of fatigue damage of asphalt mixture in the four-point bending fatigue test. And its reliability was verified by finite element simulation (Wang *et al.* 2018a). Irfan et al. established a function among the number of fatigue failure cycles, initial strain, viscosity, optimum asphalt content, and elastic modulus through a non-linear model formulation. And the results of the model could be used as a basis for selecting asphalt concrete mixtures based on fatigue life criteria (Gul *et al.* 2018). Moghaddam et al. have applied a Support Vector Machine Firefly Algorithm (SVM-FFA) method to estimate the fatigue life of asphalt pavement. And they investigated that compared with other test results, the data acquired from this method was more accurate (Moghaddam *et al.* 2016). However, none of these theoretical prediction models could reflect the real real-time fatigue development process of asphalt pavement.

With the application of artificial intelligence technology in road engineering, many researchers have used intelligent detection technology to test the performance and

distress of pavement structure. Currently, the fibre Bragg grating is one of the most widely used intelligent detection technologies. Researchers have applied it to the quality control and structure health monitoring of road engineering (Zhou *et al.* 2012, Yiqiu *et al.* 2014, Carey *et al.* 2017, Wu *et al.* 2019). Although fibre Bragg grating was widely used in road engineering, its layout was complex, and its survival rate remained low (Fielder *et al.* 2004, Burunkaya and Yucel 2020). Li et al. proposed a crack classification algorithm based on interleaved low-rank group convolution hybrid deep network (ILGCHDN) to evaluate pavement's structural damage by calculating the crack area (Li *et al.* 2021). To detect the asphalt concealed damage, Ji et al. embedded lead zirconated titanite/polyvinylidene fluoride composite aggregate (CPA) into asphalt pavement and established a relationship model between root mean square deviation (RMSD) and crack width using amplitude attenuation as a monitoring index (Ji *et al.* 2019a). After that, Ji et al. used piezoelectric ceramics to find that the attenuation coefficient of acoustic waves decreased with the increase of pavement crack width, which proved the feasibility of using wireless sensing technology to monitor the development of pavement crack (Ji *et al.* 2019b). Hasni et al. developed battery-free wireless sensors with non-constant injection rates that accurately detect the development of bottom-up crack of asphalt pavement (Hasni *et al.* 2017). Xue et al. developed an embedded sensing network for pavement health monitoring. The pavement responses collected by the sensor network were used to predict the long-term performance of the pavement and serve as a basis for subsequent pavement management (Xue *et al.* 2014). However, the accuracy of structure health monitoring is affected by the environment. Hu et al. minimized the influence of environment on the process of structural health monitoring based on Principal Components Analysis (PCA) methods (Yan *et al.* 2005, Hu *et al.* 2012).

In the process of compaction and service of asphalt pavement, aggregate rotates and displaces under the effect of external force, resulting in the rearrangement of the mixture and eventually leading to the reinforcement of the skeleton structure of the mixture. However, when the ultimate bearing capacity is exceeded, coarse aggregate is broken, resulting in the skeleton's instability, leading to pavement structural distresses. To study the movement of coarse aggregates during compaction, Shi et al. used image processing methods to investigate the correlation between aggregates movement and rutting resistance (Shi *et al.* 2020). Li et al. used CT scanning technology to confirm that the densification characteristics of asphalt mixture were closely related to the displacement of coarse aggregates during rotary compaction (Li *et al.* 2019). In addition, Gong et al. used numerical simulation technology to find that aggregates of different shapes had different motion characteristics during SGC rotating compaction (Gong *et al.* 2018). To obtain the movement of real aggregates, Wang et al. simulated real aggregate movement through SmartRock and obtained the movement of aggregate in the process of compaction in real-time. The results showed that the aggregate movement was highly correlated with the development of the asphalt mixture's compactness (Wang *et al.* 2018c, Wang *et al.* 2019, Dan *et al.* 2020). And the application of Intelligent Aggregate (IA) developed by Zhang in the compaction process also showed that the correlation between compaction degree, spatial attitude angle, and spatial acceleration is significant (Zhang and Wang 2021). Furthermore, Erdem et al. compared X-ray computed tomography images before and after the HVS rut test. They found a significant aggregate movement in the direction of travel and the underside of the driven wheel. Significant differences in aggregate movement and void variation were also observed between overlay thicknesses (Coleri *et al.* 2012). These studies showed that the movement of aggregate in asphalt mixture is closely related to its functional and structural performance.

123 The researchers found that any particle's motion starts with a rotation, a process
124 perhaps accompanied by a linear displacement (Wang *et al.* 2018c). Under repeated load,
125 the fatigue failure and permanent deformation of asphalt pavement are also accompanied
126 by the rotation and displacement of coarse aggregate. Therefore, this paper starts from the
127 movement characteristics of aggregate under the action of load, uses intelligent sensing
128 technology to obtain its kinematic response signal, and explores the kinematics law of
129 aggregate. The kinematic response under repeated load could reflect the fatigue
130 development of asphalt mixture to realize the purpose of real-time monitoring of asphalt
131 mixture performance under long-term load. The study of acceleration and angle signal
132 variation is envisaged to explain the fatigue development of asphalt pavement structure
133 under repeated vehicle loads from an entirely new perspective.

# 134 2 Materials and methods

135 In view of the integral nature of the movement of the asphalt mixture specimen
136 under loading, the sensor was supported in the form of a patch attached to the specimen's
137 surface to obtain the kinematic response of the specified parts of the specimen under
138 fatigue loading.

## 139 *2.1 Preparation of acceleration sensor patch*

140 A tri-axis acceleration sensor is used as the motion sensing element in this paper.
141 The dimensions and main technical parameters are shown in Fig. 1 and Table 1.

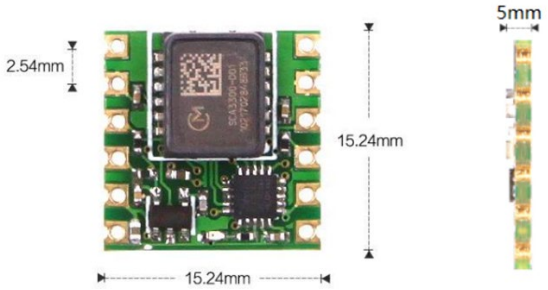


142

**Fig. 1. Tri-axis accelerometer**

**Table 1. Technical parameters of the sensor**

| Tri-axis accelerometer | |
|---|---|
| Power supply | 3.3-5v |
| Operating current | 5.5-6mA |
| Acceleration range | ±3g |
| Acceleration accuracy | ±15mg |
| Angle range | ±90° |
| Angle accuracy | 0.05° |
| Date output frequency | 10Hz |
| Module size | 15.24*15.24*5mm |

143

144 Kinematic parameters acquired from a tri-axis acceleration sensor is by converting
145 mechanical signals into electrical signals, and then converting electrical signals into
146 digital signals. After the kinematic data acquired, digital filtering techniques are used to
147 reduce data noise and improve its accuracy. And Biphasic Dose Response Function is
148 used to fit the acquired data.

149 The sensor was welded and encapsulated in a suitable mold (25mm in diameter).
150 The self-developed sensor patch is shown in Fig. 2. The sensor patch was bonded to the
151 specimen surface while keeping the surface clean and flat to make the contact surface
152 neatly bonded, thus improving the test accuracy.

153 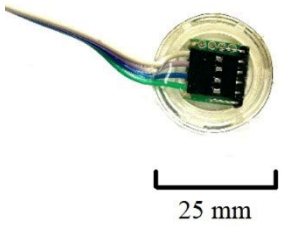


**Fig. 2. Acceleration sensor patch**

154 ***2.2 Fatigue loading test***

155 To better simulate the actual stress condition of asphalt pavement structure and
156 simplify the test process, the SCB fatigue test was adopted to study the fatigue
157 performance of the asphalt mixture, and the gradation of asphalt mixture was SMA-13.
158 The Universal Testing Machine (UTM-30) multi-functional testing machine was adopted
159 as the fatigue test instrument.

160 The middle position of the bottom of the SCB specimen (150mm in diameter and
161 50mm in thickness) is the main tensile area of the whole specimen, which is the critical
162 location for the first fatigue failure and the occurrence and development of cracks. It is
163 also the main area determining the primary axis displacement of the UTM-30 application
164 point in the fatigue test. Therefore, studying the movement characteristics of aggregate in
165 this area is of great significance.

166 In the process of the SCB fatigue test, the pressure head of UTM-30 had an impact
167 on the whole specimen. Under loading, the instantaneous compressive stress is generated
168 in the upper part of the specimen, and the instantaneous tensile stress is generated in the
169 lower part of the specimen, accompanied by the bending deformation at the bottom.
170 Asphalt mixture has viscoelastic properties. At the moment of unloading, the load-
171 deformation generated by the specimen recovers at the fastest speed at the corresponding

viscoelasticity level of the asphalt mixture. At this moment, the stress changes at the top and bottom of the specimen, upside by compression transformation for the tension, lowering the tension into compression, shown in Fig. 3. During the whole loading and unloading cycle, the specimen produces shock and rebound acceleration in the loading direction.

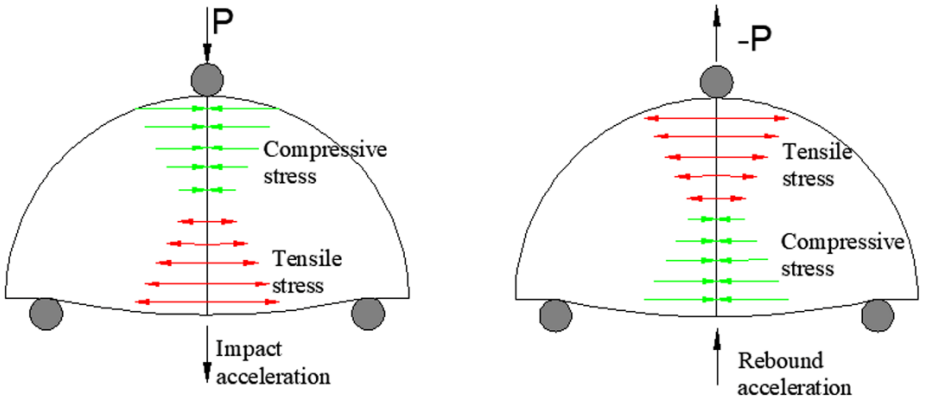


**(a) Load** **(b) Unload**

**Fig. 3. Stress distribution of semi-circular bending specimen**

### *2.3 Position selection and calibration of acceleration sensor patch*

Currently, channelized transportation is adopted to optimize transportation mobility and efficiency and reduce traffic accidents. However, channelized traffic following the designated route pattern leads to severe distresses such as rutting/ permanent deformation in the track belt.

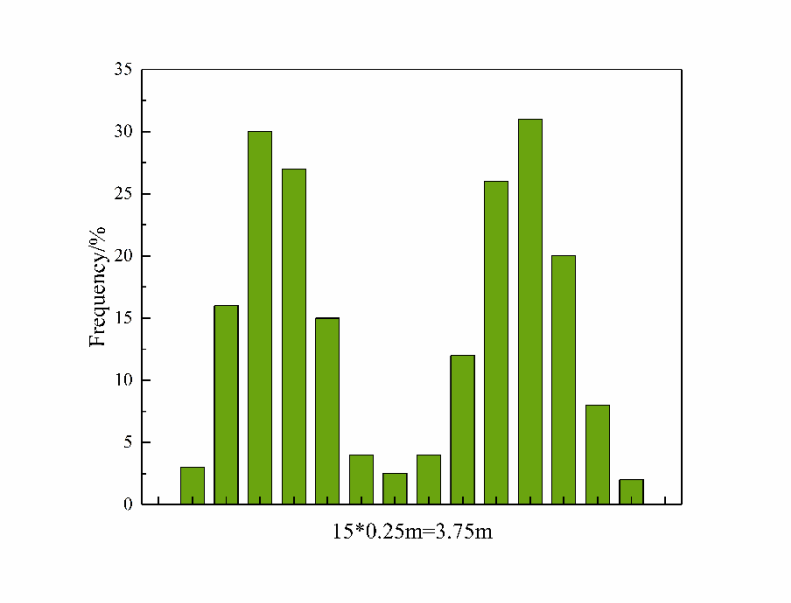


**Fig. 4. Vehicle wheel track distribution frequency**

Fig. 4 shows the distribution frequency of wheel tracks around the 3.75m road track belt under a wheel load. It is evident that the distribution of wheel track frequency decreases gradually from the tire centre to both sides under load. Due to the structural integrity of the asphalt pavement, the tire also affects the uncontacted (track belt edge) pavement around it.

In the process of studying the fatigue performance of asphalt mixture, we should not be limited to the stress condition under the load but take the influence of the load on the surrounding wheel track into account. When the vehicle load does not act directly above the embedded sensor on the pavement, the aggregate could still respond to the influence of the vehicle load on the pavement structure to a certain extent. To obtain the motion parameter responses and changes of the acceleration sensor patch at different positions of the specimen, three positions of the SCB specimen were selected, as shown in Fig. 5.

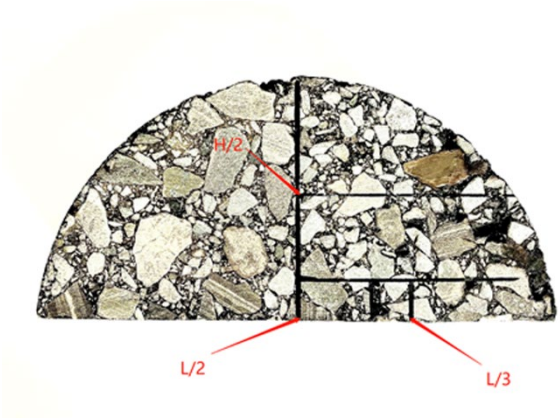


197

**Fig. 5. Position of the acceleration sensor patch**

198 The sensor patch and the position of the bottom half of the semi-circular specimen
199 (L /2), the lower third of the right part (L /3), and the vertical half of the middle part (H
200 /2) are placed, respectively. Three tests at different positions are set as a group, and the
201 SCB specimens in each group are all from the same cylindrical specimen. The test is
202 repeated three times for each position to verify the repeatability test. The patch mode and
203 coordinate axis of the sensor on the specimen surface are shown in Fig. 6.

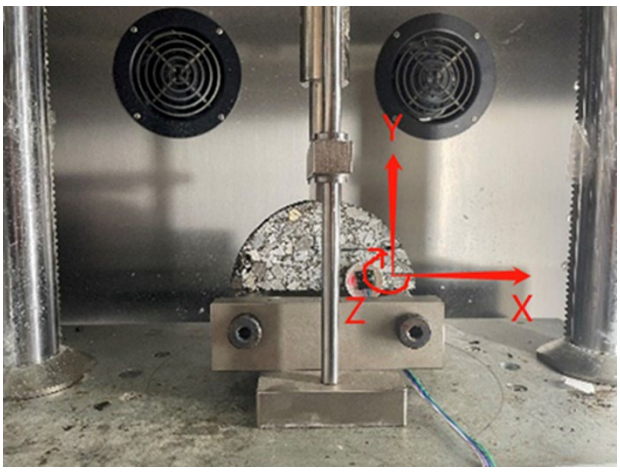


204

**Fig. 6. Sensor coordinate axis**

205 ***2.4 Determination of loading mode and stress ratio***

206 In this study, the intermittent rectangular load is adopted, it can simplify the stress
207 analysis of the specimen. The loading frequency is determined as 1Hz, that is, 0.1s

208 loading and 0.9s intermittent rest period, to ensure that the sensor patch can have enough
209 reaction time. The data collection time of the sensor in this test is set at ten times per
210 second.

211 To select an appropriate stress ratio and comprehensively consider the accuracy
212 and efficiency of test results, two ultimate bearing capacity tests are conducted on semi-
213 circle specimens at a temperature of 15℃, as shown in Fig. 7. Its average value is taken
214 as the ultimate bearing capacity of the specimens, and the failure load is 13.28 kN. The
215 stress ratio of the semi-circle bending fatigue test is 0.14, and the load level is 1.8 kN.

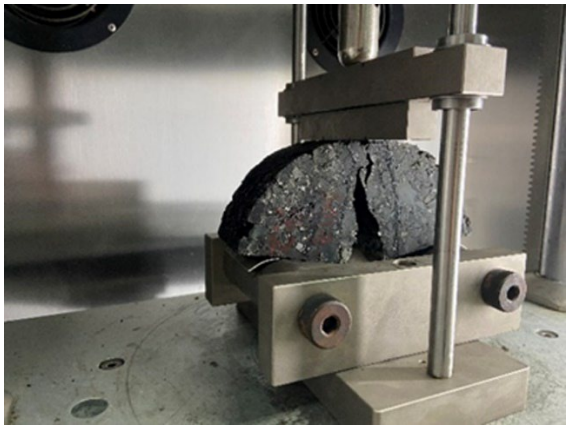

216

**Fig. 7. Ultimate bearing capacity test**

# 217 3 Results and Discussion

## 218 *3.1 Investigation of fatigue test results*

219 Fig. 8 shows the displacement development curve of the semi-circle specimen at
220 the point of an application under cyclic load. At the point of application, the spindle
221 displacement presents a reverse S-shaped development until the SCB specimen is
222 damaged.

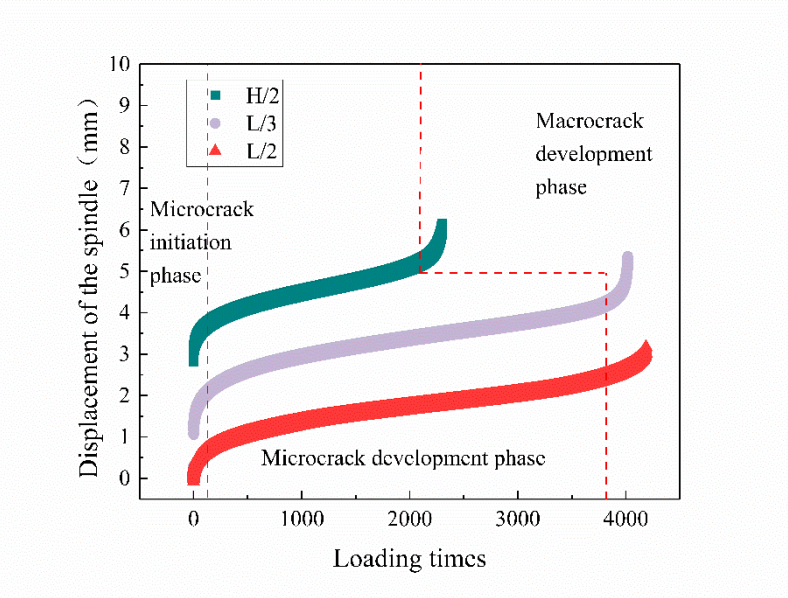


**Fig. 8. Spindle displacement curve**

As can be seen in Fig. 8, in this process, the spindle displacement curve has two inflection points. The fatigue damage process conforms to the law of the three stages of evolution, the micro-crack initiation stage, the micro-cracks expansion stage, and the macroscopic crack extension stage. The second phase experiences the longest time. Therefore, this stage is essential for studying the fatigue evolution law. The third stage of specimen failure is a concrete manifestation of fatigue damage accumulation in the second stage.

At the end of the fatigue test, we find that the aggregates at the fractures are intact, and some of the aggregates have asphalt attached to the surface, as shown in Fig. 9. This phenomenon indicates that fatigue damage occurs mainly in the fatigue fracture of the asphalt-aggregate bond and of the asphalt itself. The results show that the fatigue performance of asphalt mixes is mainly influenced by the adhesion between asphalt and aggregate and the surface tension caused by the viscoelasticity of the asphalt itself.


237

**Fig. 9. Fracture of the sample**

238 ***3.2 Analysis of acceleration and angle changing characteristics***

239 Fig. 10, 11, and 12, respectively show the acceleration changes at L/2, H/2, and

240 L/3 position obtained by the sensor patch during the fatigue test.

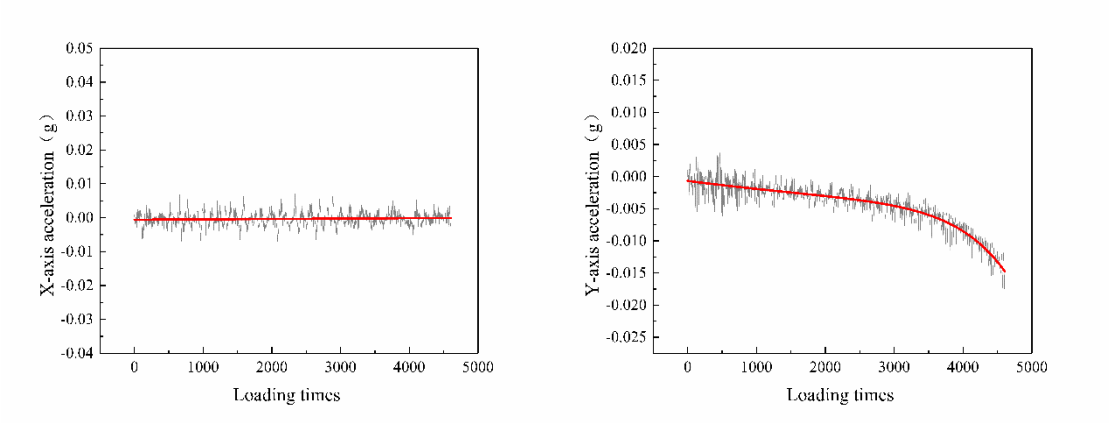


241

**(a) Change in X-axis acceleration** **(b) Change in Y-axis acceleration**

242

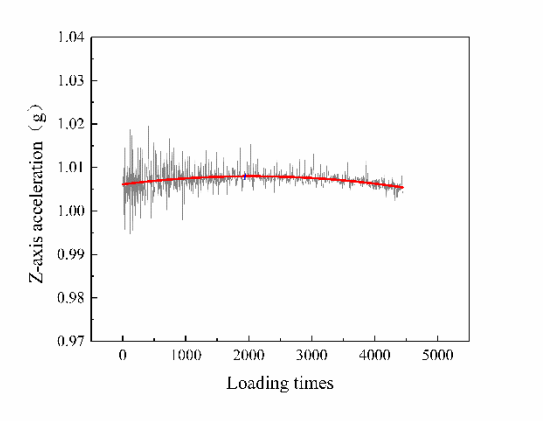


243

**(c) Change in Z-axis acceleration**

**Fig. 10. Acceleration changes at L/2 position**

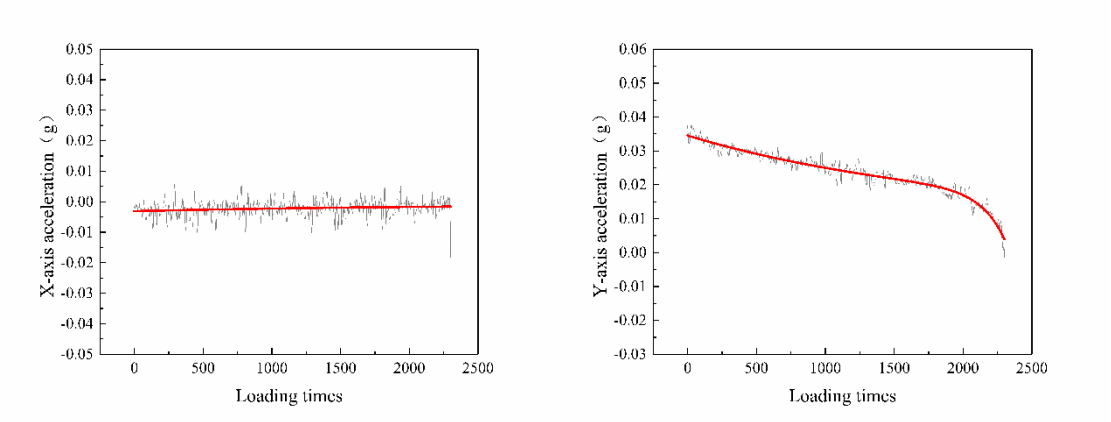


**(a) Change in X-axis acceleration** **(b) Change in Y-axis acceleration**

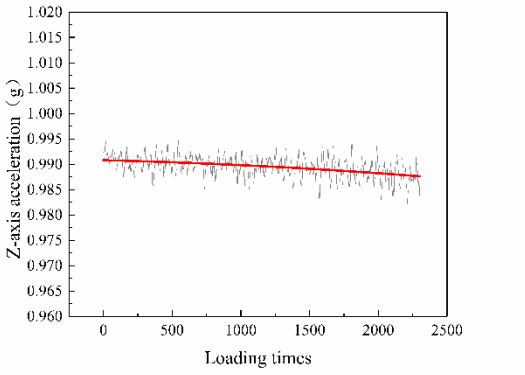


244

**(c) Change in Z-axis acceleration**

**Fig. 11. Acceleration change at H/2 position**

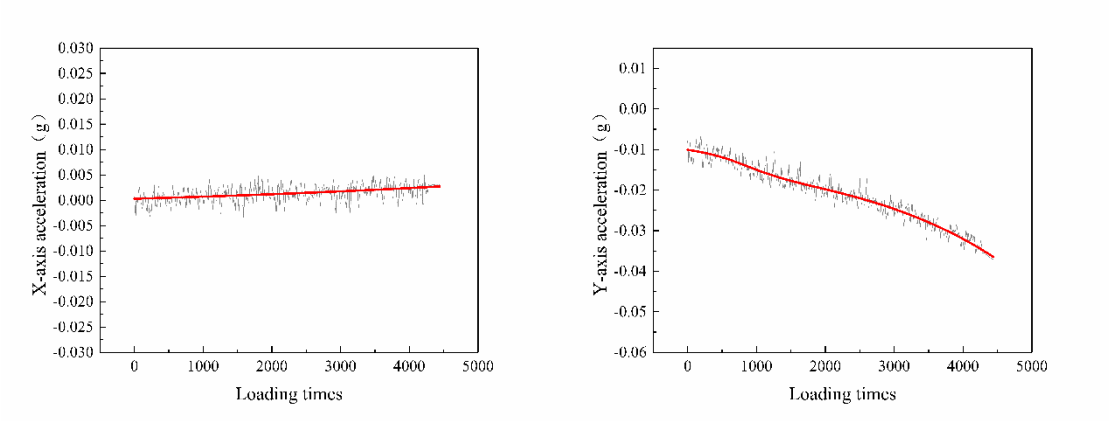


**(a) Change in X-axis acceleration** **(b) Change in Y-axis acceleration**

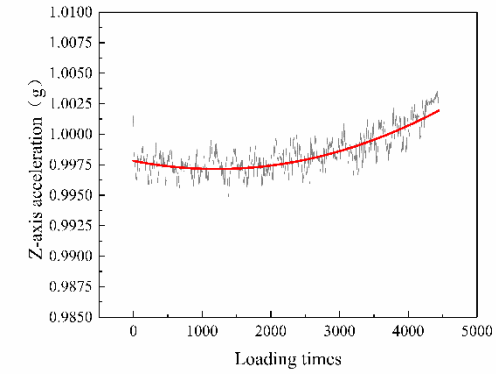


**(c) Change in Z-axis acceleration**

**Fig. 12. Acceleration change at L/3 position**

The sensor patch at the three positions has different changes in all three directions. The acceleration changes along the X direction are the same in the three stages at three positions during the SCB fatigue process. During the whole test process, the acceleration fluctuates around 0, and the fluctuation is in a relatively stable state. But the acceleration fluctuation at the L/3 position is more slightly than the other two positions. The X-axis is the coordinate axis parallel to the bottom edge of the SCB specimen. During the interconversion of tensile and compressive stresses in the specimen under load, the conversion between shock acceleration and rebound acceleration shows a corresponding situation, which can be taken as the specimen's response to tensile forces in the X-axis

direction. As a result, the acceleration in the three directions (i.e., the acceleration resulting from the interconversion of tensile and compressive stresses parallel to the level of the specimen during loading and unloading) shows steady fluctuations throughout the fatigue test. Because the L/3 position is not in the central area where tension and compression vary, the acceleration fluctuation is much smaller than in the other two positions. The results show no significant trend in the acceleration response to the whole process at different positions under a wheel load. In contrast, the acceleration response is most pronounced at positions below the wheel track. The Y-axis acceleration at all three different positions shows a clear parabolic trend, which means that the shock acceleration plays a dominant role in the process. Throughout the microcracking phase and in the early stages of microcrack development, shock and rebound accelerations alternate with large values, except at the H/2 position. The variation in acceleration on the Y-axis can be explained by the excellent viscoelastic properties of the asphalt mix in the early stages of loading, with strong adhesion between the asphalt and the aggregate surface. As a result, its elastic rebound is good when loaded. Most of the specimens are deformed elastically and recover in a very short time (0.9s interval) after unloading, and as a result, vertical shock acceleration and rebound acceleration vary. This phenomenon occurs in the early stages of fatigue damage, i.e., during the crack initiation and microcrack development stages. However, after passing through the early stages of the second fatigue damage phase, internal damage to the asphalt mix structure has occurred, accompanied by a decrease in the viscoelasticity, surface tension, and modulus of elasticity of the asphalt binder. Under the same load, the partial elastic deformation of the asphalt mix gradually transitions to plastic deformation. Thus, this stage of the deformation by plastic and elastic deformation is two kinds of deformation. The rebound deformation of resilience provided that is reduced to make the rebound acceleration decrease. After unloading, due to the

strong plasticity of the asphalt mixture in this phase and its reduced viscoelasticity, the rebound deformation of the specimen requires more time to recover, resulting in the lagging of the specimen rebound deformation, thus not enabling the specimen to rebound to the initial state. During the recovery of deformation, the next loading has already occurred, i.e., when the shock acceleration has not recovered to zero, the next loading causes the shock acceleration generated by the specimen to superimpose on the previous residual shock acceleration, eventually leading to a situation where the shock acceleration becomes increasingly large. When the fatigue damage enters the third stage, the Y-axis acceleration and displacement of the spindle develop very similarly. Upon entering this phase, the acceleration and displacement of the spindle accelerate, cracks appear in the specimen and gradually extend towards the middle of the specimen, the integrity of the asphalt mix is destroyed, and the change in acceleration stops. There are still significant differences between the three positions. As the loading time increases, although the average acceleration values of the three positions gradually decrease, the acceleration at position H/2 shows a clear triadic variation, which is more conspicuous than in the other two positions. The lower part of the SCB specimen is the tensile zone, and the stress is subjected to tensile stress. At the H/2 position, the sensor patch is arranged at the vertical midpoint of the SCB specimen, in the region where tensile stress and compressive stress act together, so its stress state is more complex than that of the middle and lower parts. The L/2 and H/2 position acceleration significantly differ before the later stages of fatigue development. This phenomenon can be interpreted as the upper specimen in the cutting plane perpendicular to the semi-circular reference a lower amount of expansion under the same load. As a result, viscoelastic attenuation of the asphalt at the upper part of the specimen under cyclic load has not reached the point where the accelerated change in this direction produced an obvious difference. At the L/3 position, because the sensor patch

at this position is not located directly under the load, it is subjected to a certain eccentric force, so the regularity of its performance is not as good as the acceleration change of the sensor patch at two positions directly under the load. The effect of the fatigue load is somewhat weaker at this position than at the other two positions. In the Z-axis direction, the acceleration variations at the initial and final stages at the three positions show some differences. Acceleration at the L/2 position fluctuates more strongly at the initial stage and becomes stable slowly when the process goes to the middle part. In contrast, acceleration at the L/3 position keeps stable at the pre-middle stage. It increases steadily in the later stage, which indicates that the rebound acceleration plays a more important role than shock acceleration at this position in the later stage. And acceleration at H/2 remains stable through the whole test. Throughout the loading process, the stress state along the Z-axis of the semi-circular specimen is similar to that of the specimen in the indirect tensile test. Under a vertical load, the specimen developed deformation and stresses perpendicular to the direction of the load. The test exhibits mainly expansion and contraction perpendicular to the direction of the semi-circular cutting surface of the specimen. Again, the expansion and contraction of the specimen are influenced by the viscoelasticity of the asphalt mixture. With the increase of load cycles, asphalt mixture shows stress relaxation phenomenon, and the elastic deformation of asphalt mixture specimen part into plastic deformation, which made the expansion of the specimens after loading quantity decrease, eventually leading to shrinkage and shrinkage rate after unloading is reduced. As a result, the shock acceleration and rebound acceleration in the Z-axis direction is gradually reduced.

In the fatigue test process, the deformation of specimens produces not only the change of acceleration but also the change of angle. As one of the parameters for evaluating the movement of asphalt mixture specimens, the angle also shows a certain

regularity, as shown in Fig. 13, 14, and 15. As the Z-axis direction is perpendicular to the semi-circular cutting surface of the specimen and the loading direction, the angular change in this direction during the test is 0. Therefore, the angular change in this direction is not discussed, and only the angular change in the X- and Y-axis directions are analysed.

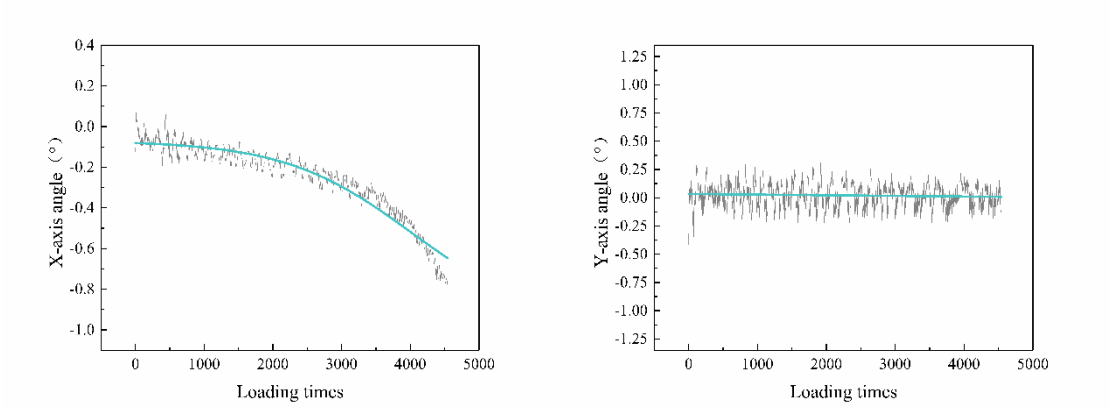


**(a) The X-axis Angular change** **(b) The Y-axis Angular change**

**Fig. 13. Angular change at the L/2 position**

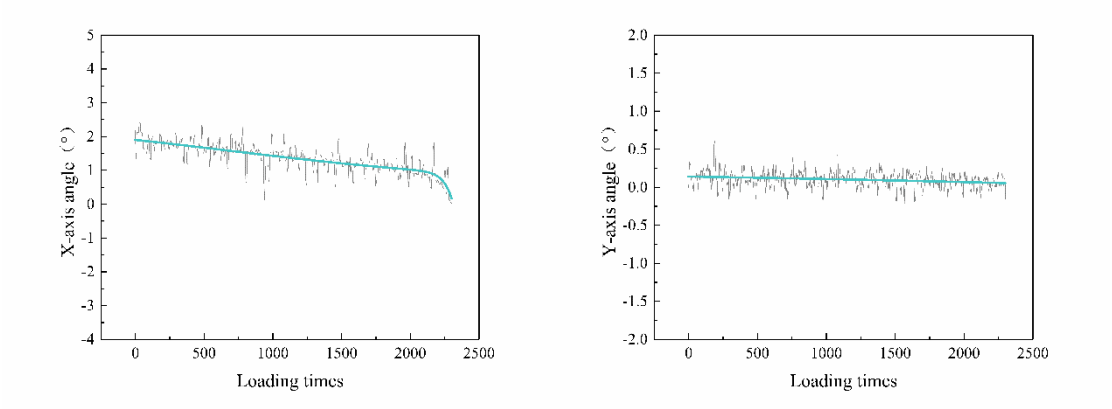


**(a) The X-axis Angular change** **(b) The Y-axis Angular change**

**Fig. 14. Angular change at the H/2 position**

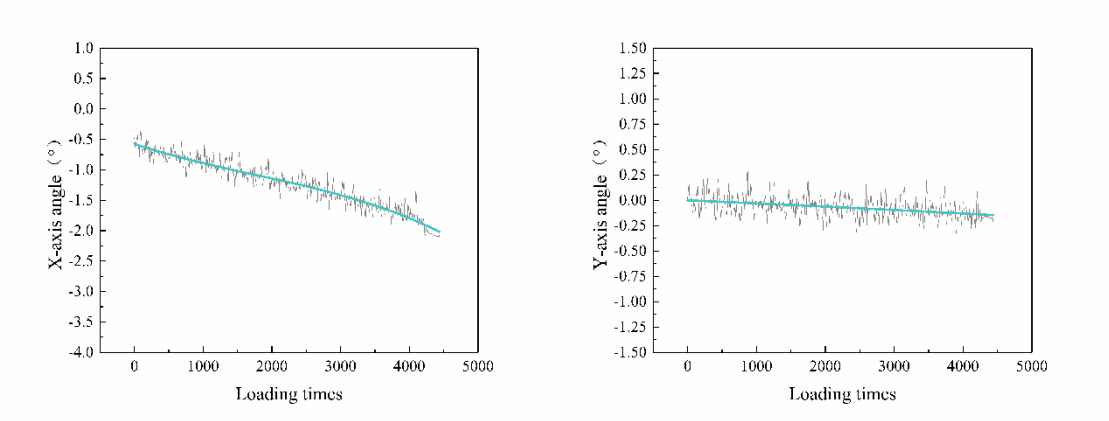


**(a) The X-axis Angular change** **(b) The Y-axis Angular change**

**Fig. 15. Angular change at the L/3 position**

The angular changes at the three positions show almost the same trend but significant differences in the two directions. It is worth noting that the change in acceleration on the Y-axis and the change in angle on the X-axis show the same trend, both showing a downward parabolic trend. And the angular change in Y-axis at three positions maintains stability in the real test. In the X-axis direction, as it is parallel to the bottom of the semi-circular specimen, it reflects the straight line at the centre of the bottom and the change in angle between the horizontal plane and the pivot point of the specimen. As the test proceeds, and as the number of loads increases, some of the specimen's elastic deformations gradually transform into plastic deformation, causing permanent deformation at the bottom of the specimen, which cannot be restored to its initial state. Therefore, the angle of its X-axis gradually accumulated and became more significant. However, the decrease of viscoelasticity and the accumulation of plastic deformation made the resilience of asphalt decrease gradually, showing that the difference between the maximum and minimum angular changes becomes larger. The angle changes along the Y-axis indicate that the specimen under the load action does not produce obvious

deformation and stress change in this direction, so the angle along the Y-axis before and after the test does not produce a noticeable change.

In summary, the kinematic response of sensor patches at all three positions of the semi-circular specimen reflects the changes in the fatigue performance of the asphalt mix in the fatigue test. The changes in acceleration of the sensor patch on the Y-axis and the changes in angular on the X-axis are the most similar to the displacement development curve at the application point.

### *3.3 Determination of optimum fatigue response position and index*

From the above analysis, it can be clear that the acceleration variation trend of each part along the Y-axis and the angle variation trend along the X-axis are similar to the development trend of the spindle displacement (vertical deformation). To further quantify the degree of correlation among the three, origin is used to carry out curve fitting for the three data and then works out the negative number of the data on the curve of acceleration and angle change. The results are shown in Fig. 16.

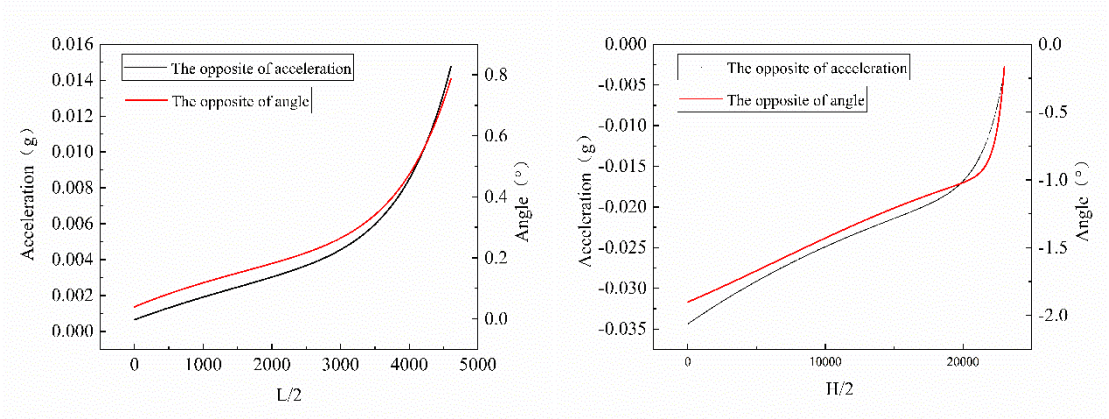


**(a)** **(b)**

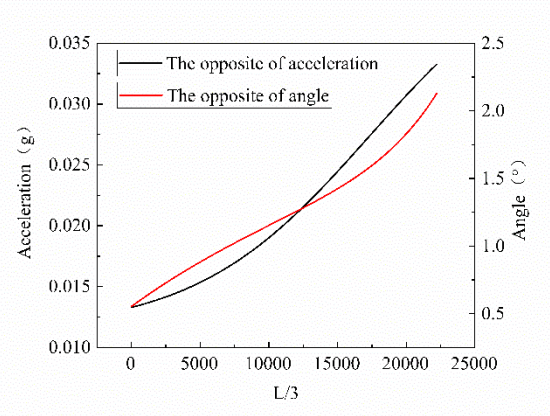


368

369 **(c)**

**Fig. 16. Negative of the acceleration and Angle change curve**

370 Finally, Pearson correlation analysis on the three was carried out. The results are

371 shown in Fig. 17, indicating that the correlation among the three was significant.

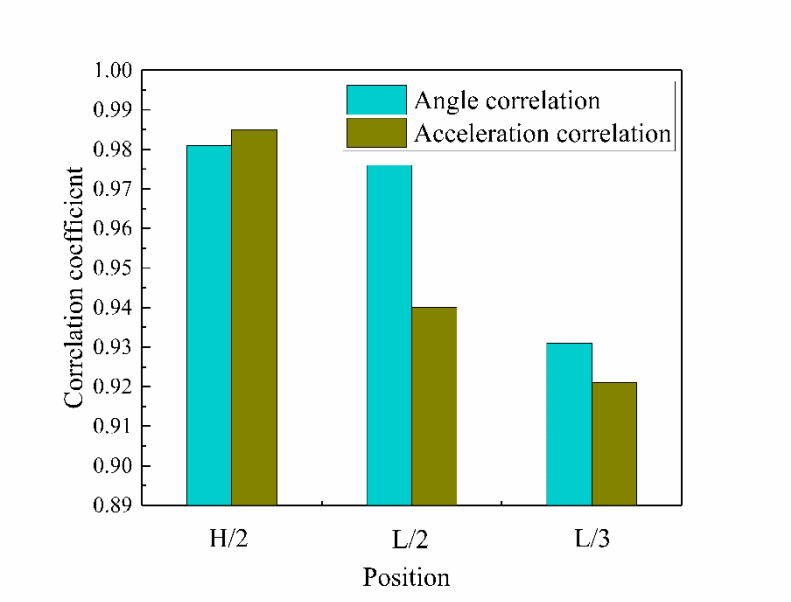


372

**Fig. 17. Correlation between different positions of SCB specimens and their kinematic characteristics**

373 It can be seen that the correlation between the angle variation curve and the

374 displacement development curve, as well as the correlation between the acceleration

375 variation curve and the displacement development curve, are above 0.91. The relationship

between the asphalt mixture kinematic parameters and its axial displacement can represent the change in asphalt mixture fatigue performance. This relationship also confirms the feasibility of the sensor patch in monitoring the fatigue performance of asphalt pavements and reflects the solid guiding significance of this study for engineering practice. Variations in the angle and acceleration profiles of the semi-circular specimens with the sensor patch in different positions can also be found. The development of the displacement curve has a different relationship with the highest overall performance correlation when the sensor patch is located at H/2, followed by L/2. The worst correlation is when the specimen L/3 sensor patch is halfway down. Under actual pavement loading conditions, it is at a certain structural depth directly below the track belt. The deeper the sensor is buried, the poorer the accuracy of the parameters obtained to reflect the fatigue performance of the pavement. Therefore, in practical engineering applications, the burial depth of the sensing facilities should be reasonably controlled. Its significance is weakened when the accelerated patch is placed on either side of the track belt. In other words, the effectiveness of the reflection of the fatigue performance of the asphalt pavement has further deteriorated. Although the effect of sensors at different locations on the fatigue performance is different, the accuracy of the sensors is greatly improved if the kinematic parameters obtained from different locations are combined to form an array of sensing facilities in the pavement structure.

Although the acceleration and angle changes indicate the decay in pavement fatigue performance, there are still significant differences between them. As can be seen from the previous analysis, the angle change curve is more clearly correlated with the force point displacement development curve than the acceleration development curve is with the force point displacement development curve, although they are close to each other at H/2. Changes in angle are therefore more suitable for monitoring the fatigue

401 performance of pavements than changes in acceleration. In addition to this, vehicle loads
402 are not constant in actual asphalt pavement use, and the loading frequency is not uniform.
403 It is assumed that acceleration is used as the best evaluation indicator. In this case, it only
404 reflects the rapid movement of the pavement under vehicle loading, and of course, the
405 rebound acceleration, which is the total long-term load, is significantly attenuated.
406 However, it is only applicable to pavement fatigue performance after significant
407 attenuation and not to monitoring pavement fatigue performance during short to medium-
408 term use.

409 For the angle of the sensor, the elastic deformation of the pavement structure of
410 the asphalt pavement is gradually transformed into plastic deformation under long-term
411 loading, resulting in permanent deformation of the pavement structure and changing the
412 angle of the accelerated patch. This change accumulates gradually and permanently and
413 is not affected by the action of wheel loads. It can therefore record the change in angle of
414 the aggregates in the pavement structure in real time and permanently, enabling the
415 recording of movement parameters over the whole life cycle of the pavement and
416 reflecting the fatigue decay of the pavement structure. To further analyse the change of
417 the aggregate angle in the fatigue loading process, the derivative fitting of the X-axis
418 angle at the H/2 position and its displacement development curve was carried out, as
419 shown in Fig. 18. The relationship between the Angle-Accumulation-Rate (AAR) and the
420 accumulation rate of the spindle displacement was studied.

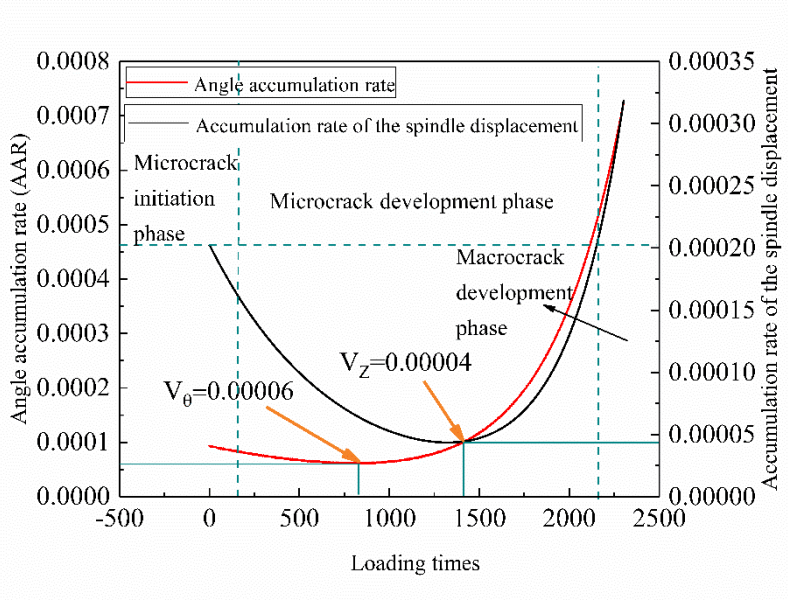


421

**Fig. 18. Comparison of cumulative rate of angle and spindle displacement**

422 At the microcrack initiation stage, the spindle has a high displacement
423 accumulation rate of approximately 0.0002 and an AAR of approximately 0.0001. As the
424 development enters the micro fatigue crack growth stage, the point accumulation rate and
425 spindle displacement accumulation rate gradually decrease. When the number of loads
426 reaches about 800, the AAR drops to a minimum of 0.00006. The spindle displacement
427 is still falling, and the cumulative rate drops to a minimum of roughly 0.00004 when the
428 number of loads reaches about 1400. they reach the minimum point 600 times apart; when
429 the cumulative rate of spindle displacement reaches a minimum, the AAR returns to
430 0.0001, where the first intersection of the two occurs. After that, the AAR and the
431 cumulative rate of spindle displacement increased rapidly as the number of loads
432 increased. When the number of loads reaches approximately 2200, the cumulative rate of
433 spindle displacement increases to approximately 0.0002, the same as the initial time. At
434 this point, a macroscopic crack appears at the bottom of the SCB specimen and begins to
435 enter the macroscopic crack extension stage. At this point, the AAR is approximately
436 0.0005, which is twice the rate of spindle displacement accumulation.

The results show that when the AAR in the Y-axis is in the decreasing phase, the asphalt pavement is in an excellent state of performance. However, as the number of axial loads increases, the AAR gradually increases. When it increases to 0.0005, the asphalt pavement is expected to suffer structural damage. Therefore, when the AAR reaches ten times that of the AAR at the inflection point in the whole stage, as shown in Equation (4), it is considered that apparent damage has occurred to the asphalt pavement and early warning and maintenance plans should be made.

$$V_c = 10V_i \tag{4}$$

Where, $V_c$ is the AAR when the asphalt mixture enters the macro-crack growth stage; $V_i$ is the AAR at the inflection point in the fatigue development process of asphalt mixtures.

# 4 Conclusions

This paper evaluated the asphalt mixture fatigue phenomenon using the SCB fatigue test method. The integral kinematic characteristics of the aggregate in the specimens under the load is utilized. A square wave is used as a fatigue loading method to simplify the specimen stress distribution and amplify the self-developed sensor signal obtained by movement. The relationship between the variation of kinematic response and the development of the displacement of the application point during the fatigue loading process is analysed, and the main conclusions are as follows:

Fatigue cracks of asphalt mixture specimens mainly appear in the asphalt itself and on the bonding surface of aggregate and asphalt. The attenuation of asphalt viscoelasticity and the surface tension between asphalt and aggregate during the test lead to the variation of kinematic response in three directions. The transformation of elastic

deformation to plastic deformation of the test specimen results in the accumulation of X-axis rotation angle and Y-axis shock acceleration, having a similar three-stage changing trend.

The position of the sensing facility dramatically influences the accuracy of fatigue kinematic response. Correlation analysis shows that the correlation between the change curve of angle and acceleration at H/2 and the change curve of displacement at the application point is the largest, reaching 0.981 and 0.985, which can better reflect the fatigue property attenuation of asphalt mixture in the process of fatigue test, followed by the position of L/2 of the specimen. Kinematic response of aggregate at L/3 position has the worst reflection on the attenuation of asphalt mixture's fatigue performance. Therefore, the position of the sensing facility in the pavement on the field should be reasonably considered to obtain the ideal data. However, because of the permanent nature of angle accumulation and the transient nature of acceleration response, angle variation is more suitable than acceleration variation for long-term fatigue performance monitoring of asphalt mixtures under vehicle load.

The novel Angle Accumulation Rate (AAR) is presented as the real-time and long-term fatigue performance monitoring index of the asphalt mixture. By comparing the development curve of spindle displacement accumulation rate and AAR, the asphalt pavement is considered damaged when the AAR at the upper-middle point of semi-circular specimen approaches ten times the AAR curve at the inflection point – the triggering point of preventive maintenance treatment to arrest pavement structural damage.

This paper proposes a new method for monitoring the fatigue performance of asphalt mixtures by combining modern intelligent sensing and signal processing technology and traditional test methods. It is worth mentioning here that this method can

effectively predict the development trend of fatigue performance of asphalt mixtures through aggregate mesoscopic motion. The proposal of AAR also creatively combines the long-term kinematic behaviour and mechanical behaviour of asphalt mixture structure to provide effective data and theoretical support for the life cycle management of asphalt pavement. However, a wired sensor was used in this test, and the transferability and integrity of motion were utilized to study the kinematic response of the asphalt mixture specimens. In future research, it is possible to turn wired sensors into wire-less sensors by optimizing the sensor transmission mode. And shaping the appearance of the sensing facility by effective encapsulation to an aggregate-like size and shape, which makes the sensing facility could be used as the skeleton of the asphalt mixture to obtain a more accurate kinematic response.

# 5 Disclosure statement

No potential conflict of interest was reported by the authors.

# 6 Funding

This research was supported by the National Key Research and Development Program of China (No. 2021YFB2601000), the National Natural Science Foundation of China (NSFC) (No. 52078048, 51878063). The authors are solely responsible for the content.

# 7 References

Burunkaya, M. & Yucel, M., 2020. Measurement and control of an incubator temperature by using conventional methods and fiber bragg grating (fbg) based temperature

sensors. *Journal of Medical Systems,* 44 (10).

Carey, C., Obrien, E.J., Malekjafarian, A., Lydon, M. & Taylor, S., 2017. Direct field measurement of the dynamic amplification in a bridge. *Mechanical Systems and Signal Processing,* 85, 601-609.

Coleri, E., Harvey, J.T., Yang, K. & Boone, J.M., 2012. Investigation of aggregate movement and air-void reduction on heavy vehicle simulator test sections by computed tomography imaging. *Cies Research Paper*.

Dan, H.-C., Yang, D., Liu, X., Peng, A.-P. & Zhang, Z., 2020. Experimental investigation on dynamic response of asphalt pavement using smartrock sensor under vibrating compaction loading. *Construction and Building Materials,* 247.

Dong, Q., Zhao, X., Chen, X., Ma, X. & Cui, X., 2020. Long-term mechanical properties of in situ semi-rigid base materials. *Road Materials and Pavement Design*, 1-16.

Du, Z.Y., Yuan, J., Xiao, F.P. & Hettiarachchi, C., 2021. Application of image technology on pavement distress detection: A review. *Measurement,* 184 Available from: <Go to ISI>://WOS:000704796600001.

Fielder, R.S., Klemer, D. & Stinson||agby, K.L., Year. High neutron fluence survivability testing of advanced fiber bragg grating sensorsed.^eds. *Aip Conference*.

Gong, F.Y., Zhou, X.D., You, Z.P., Liu, Y. & Chen, S.Y., 2018. Using discrete element models to track movement of coarse aggregates during compaction of asphalt mixture. *Construction and Building Materials,* 189, 338-351 Available from: <Go to ISI>://WOS:000449133200033.

Gul, M.A., Irfan, M., Ahmed, S., Ali, Y. & Khanzada, S., 2018. Modelling and characterising the fatigue behaviour of asphaltic concrete mixtures. *Construction and Building Materials,* 184, 723-732.

Guo, X., Sun, M., Dai, W., Zhu, K. & Li, J., 2017. Research on the fatigue whole life of

asphalt mixture based on the nonlinear damage theory. *Construction & Building Materials,* 156 (dec.15), 546-554.

Hasan, M.M., Ahmad, M., Hasan, M.A., Faisal, H.M. & Tarefder, R.A., 2019. Laboratory performance evaluation of fine and coarse-graded asphalt concrete mix. *Journal of Materials in Civil Engineering,* 31 (11), 04019259.

Hasni, H., Alavi, A.H., Jiao, P.C., Lajnef, N., Chatti, K., Aono, K. & Chakrabartty, S., 2017. A new approach for damage detection in asphalt concrete pavements using battery-free wireless sensors with non-constant injection rates. *Measurement,* 110, 217-229 Available from: <Go to ISI>://WOS:000409151400024.

Hu, W.-H., Moutinho, C., Caetano, E., Magalhães, F. & Cunha, Á., 2012. Continuous dynamic monitoring of a lively footbridge for serviceability assessment and damage detection. *Mechanical Systems and Signal Processing,* 33, 38-55.

Ji, X., Chen, Y., Hou, Y. & Zhen, Y., 2019a. Detecting concealed damage in asphalt pavement based on a composite lead zirconate titanate/polyvinylidene fluoride aggregate. *Structural Control and Health Monitoring,* 26 (4).

Ji, X., Hou, Y., Chen, Y. & Zhen, Y., 2019b. Fabrication and performance of a self-powered damage-detection aggregate for asphalt pavement. *Materials & design,* 179, 107890.

Karami, M. & Nikraz, H., 2015. Using advanced materials of granular bra modifier binder to improve the flexural fatigue performance of asphalt mixtures. *Procedia Engineering,* 125, 452-460.

Kiplagat, C., Kaluli, J., Gariy, Z. & Mutuku, R., 2017. Review of laboratory asphalt fatigue prediction models.

Li, G., Liu, Q.W., Ren, W., Qiao, W.T., Ma, B. & Wan, J., 2021. Automatic recognition and analysis system of asphalt pavement cracks using interleaved low-rank group

convolution hybrid deep network and segnet fusing dense condition random field. *Measurement,* 170 Available from: <Go to ISI>://WOS:000607617000008.

Li, J., Li, P., Su, J., Yang, L. & Wu, X., 2019. Coarse aggregate movements during compaction and their relation with the densification properties of asphalt mixture. *International Journal of Pavement Engineering*, 1-12.

Liu, G., Jia, Y., Yang, T., Du, H., Zhang, J. & Zhao, Y., 2017. Fatigue performance evaluation of asphalt mixtures based on energy-controlled loading mode. *Construction & Building Materials,* 157 (dec.30), 348—356.

Lv, S., Wang, X., Liu, C. & Wang, S., 2018. Fatigue damage characteristics considering the difference of tensile-compression modulus for asphalt mixture. *Journal of Testing and Evaluation,* 46 (6), 2470-2482.

Moghaddam, T.B., Soltani, M., Shahraki, H.S., Shamshirband, S., Noor, N.B. & Karim, M.R., 2016. The use of svm-ffa in estimating fatigue life of polyethylene terephthalate modified asphalt mixtures. *Measurement,* 90, 526-533 Available from: <Go to ISI>://WOS:000377389600061.

Qiang, L., Lee, H.J. & Kim, T.W., 2012. A simple fatigue performance model of asphalt mixtures based on fracture energy. *Construction & Building Materials,* 27 (1), 605-611.

Shi, L.W., Wang, D.Y., Jin, C.N., Li, B. & Liang, H.H., 2020. Measurement of coarse aggregates movement characteristics within asphalt mixture using digital image processing methods. *Measurement,* 163 Available from: <Go to ISI>://WOS:000575769200009.

Wang, C., Wang, H., Oeser, M. & Hasan, M.R.M., 2021. Investigation on the morphological and mineralogical properties of coarse aggregates under vsi crushing operation. *International Journal of Pavement Engineering,* 22 (12),

581 1611-1624 Available from: <Go to ISI>://WOS:000509317400001.
582 Wang, D.H., Ding, X.H., Gu, L.H. & Ma, T., 2018a. Assessment model and virtual
583 simulation for fatigue damage evolution of asphalt mortar and mixture. *Advances*
584 *in Materials Science and Engineering,* 2018 Available from: <Go to
585 ISI>://WOS:000460287800001.
586 Wang, H., Wang, C., You, Z., Yang, X. & Huang, Z., 2018b. Characterising the asphalt
587 concrete fracture performance from x-ray ct imaging and finite element modelling.
588 *International Journal of Pavement Engineering,* 19 (3), 307-318 Available from:
589 <Go to ISI>://WOS:000423370100011.
590 Wang, X., Shen, S., Huang, H. & Almeida, L.C., 2018c. Characterization of particle
591 movement in superpave gyratory compactor at meso-scale using smartrock
592 sensors. *Construction and Building Materials,* 175, 206-214.
593 Wang, X., Shen, S., Huang, H. & Zhang, Z., 2019. Towards smart compaction: Particle
594 movement characteristics from laboratory to the field. *Construction and Building*
595 *Materials,* 218, 323-332.
596 Wu, B., Wu, G. & Yang, C., 2019. Parametric study of a rapid bridge assessment method
597 using distributed macro-strain influence envelope line. *Mechanical Systems and*
598 *Signal Processing,* 120, 642-663.
599 Xue, W., Wang, L., Wang, D. & Druta, C., 2014. Pavement health monitoring system
600 based on an embedded sensing network. *Journal of Materials in Civil Engineering,*
601 26 (10).
602 Yan, A.M., Kerschen, G., De Boe, P. & Golinval, J.C., 2005. Structural damage diagnosis
603 under varying environmental conditions—part ii: Local pca for non-linear cases.
604 *Mechanical Systems and Signal Processing,* 19 (4), 865-880.
605 Yan, K., Zhang, M., You, L., Wu, S. & Ji, H., 2020. Performance and optimization of

606 castor beans-based bio-asphalt and european rock-asphalt modified asphalt binder.
607 *Construction and Building Materials,* 240, 117951.
608 Yiqiu, T., Haipeng, W., Shaojun, M. & Huining, X., 2014. Quality control of asphalt
609 pavement compaction using fibre bragg grating sensing technology. *Construction*
610 *and Building Materials,* 54, 53-59.
611 Zhang, C. & Wang, H., 2021. A new method for compaction quality evaluation of asphalt
612 mixtures with the intelligent aggregate (ia). *Materials (Basel),* 14 (9) Available
613 from: https://www.ncbi.nlm.nih.gov/pubmed/34066502.
614 Zhou, Z., Liu, W., Huang, Y., Wang, H., Jianping, H., Huang, M. & Jinping, O., 2012.
615 Optical fiber bragg grating sensor assembly for 3d strain monitoring and its case
616 study in highway pavement. *Mechanical Systems and Signal Processing,* 28, 36-
617 49.
618